Cuspidal Redundant Robots: Classification of Infinitely Many IKS of Special Classes of 7R Robots

Durgesh Haribhau Salunkhe, Sthithpragya Gupta, and Aude Billard

***Abstract*—Redundant robots, with more degrees of freedom than required for a given task, offer enhanced dexterity but can exhibit complex kinematic behaviour in motion planning. Cuspidal robots, which can change inverse kinematic solutions without crossing singularities, have been reported to pose unique challenges for motion feasibility and repeatability. While cuspidality has been extensively studied for 3R and certain 6R robots, no formal classification exists for redundant architectures. This letter presents a systematic framework for classifying 7R wrist-partitioned redundant robots based on their cuspidal properties. The method reduces the 7R structure to a parameterized 3R equivalent via the redundant joint angle, enabling the application of established theory for cuspidal robots. Using this approach, commercially available robots are analysed and categorized as cuspidal or noncuspidal. Results show that the design offsets in commercial cobots may lead to cuspidality, which can potentially cause a nonsingular change of operation mode in collaborative applications. This classification framework provides a foundation for cuspidality-aware path planning and offers practical guidelines for designing non-cuspidal redundant robots to ensure safer and more predictable operation.**

***Index Terms*—Kinematics, Industrial robots.**

I. Introduction

REDUNDANT robots are robotic systems with more degrees of freedom (DOF) than the minimum required to achieve a given end-effector task. A robot with more than six joints, therefore, has redundancy, which provides additional flexibility to optimize various criteria such as obstacle avoidance, joint limit avoidance, and manipulability enhancement [1]. Redundant robots have found widespread applications in areas where flexibility, dexterity, and safe human-robot interaction are essential, notably in humanoid-related applications, service robotics, and collaborative manufacturing.

In particular, many commercially available redundant robots with seven revolute joints, $7R$ robots, such as the KUKA LWR iiwa 7, the Franka Emika Panda, MAiRA from Neura Robotics, and the Kinova Gen3 (7-DOF version), incorporate a *wrist sub-chain* into their architecture, and thus are called *wrist-partitioned* architectures. These robots are specifically designed to mimic human-like dexterity, making the kinematic study of this special class of robots critical. Their redundancy is typically structured as a serial $6R$ architecture for positioning and orientation, combined with an extra joint that introduces redundancy.

TABLE I
Classification of Commercial $6R$ Robots on the Basis of Their Cuspidal Properties

Sr. No	Robot	Type	Property	Year
1	Unitree Z1	Cobot	Noncuspidal	2024
2	FANUC CRX-series	Cobot	Cuspidal	2022
3	Kinova Link 6	Cobot	Cuspidal	2022
4	ABB GoFa CRB 15000	Cobot	Cuspidal	2021
5	Kinova Jaco Gen 2	Cobot	Cuspidal	2013
6	FANUC M-series	Industrial	Noncuspidal	2009
7	UR5	Cobot	Noncuspidal	2008
8	KUKA KR5	Industrial	Noncuspidal	2007

Within the broader context of robot kinematics, the concept of *cuspidal robots* is important for the path planning of robots [2]. Cuspidal robots are robots that can transition between different inverse kinematic solutions (IKS) without crossing a singularity, a phenomenon known as a *nonsingular change of solutions* [3]. While cuspidality has been studied extensively for non-redundant systems, notably $3R$ manipulators [4], [5] and more recently for certain classes of $6R$ robots [6], there is no literature available concerning cuspidality analysis of redundant robots.

One of the key observations from recent studies [6] is that a generic $6R$ robot is *almost always cuspidal*. Table I shows different commercial robots available classified according to their application and cuspidal properties. A rising trend in collaborative robots, also called cobots, led to unconventional robot designs. It has been shown that most of these robots are cuspidal, and their path planning requires special considerations. This motivates the necessity to investigate the implications of cuspidality in redundant robots. Despite the redundancy, which theoretically allows bypassing singularities through internal motion, the robot can still exhibit cuspidal properties such as nonsingular change of 'operation modes' (related to IKS, refer to Section II). The cuspidal properties of a redundant $7R$ robot can be studied as a parameterized $6R$ robot. The architecture of the $6R$ robot depends on the *arm angle* or *self-motion angle*. The arm angle is not always easy to define and interpret [7], and different methods have been proposed earlier to parameterize the redundant motion of $7R$ robot [8] such as the *shoulder-elbow-wrist* (SEW) angle.

Received 6 June 2025; accepted 22 September 2025. Date of publication 17 October 2025; date of current version 28 October 2025. This article was recommended for publication by Associate Editor C. Gaz and Editor L. Pallottino upon evaluation of the reviewers' comments. This work was supported in part by EU Project DARKO under Grant H2020 ICT-46-2020 and in part by Horizon Europe under Grant 101070596, euROBIN. *(Corresponding author: Durgesh Haribhau Salunkhe.)*

The authors are with Learning Algorithms and Systems Laboratory (LASA), École Polytechnique Fédérale de Lausanne (EPFL), 1015 Lausanne, Switzerland (e-mail: durgesh.salunkhe@epfl.ch; sthithpragya.gupta@epfl.ch; aude.billard@epfl.ch).

Digital Object Identifier 10.1109/LRA.2025.3623011

A cuspidal robot presents distinct path-planning challenges because it can exhibit a continuous, nonsingular change of IKS: two different inverse-kinematic solutions for the same end-effector pose can be connected by a joint-space trajectory that does not cross a Jacobian singularity. Consequently, a trajectory that begins on IKS 'A' can smoothly move onto IKS 'B' without triggering the usual singularity indicators. If IKS 'B' later meets joint-limit, collision, or singularity constraints, the planner may encounter an unexpected infeasibility or a loss of repeatability. This phenomenon is particularly likely on closed task-space loops that encircle cusp regions. By contrast, for a noncuspidal robot, distinct IKS are separated by singularities; the robot's operation modes (defined in Section II) are separated by singularities, so any transition between branches must pass through a singular configuration and is therefore more readily detected and handled. These topological differences explain why cuspidal behaviour complicates reliable and consistent motion planning compared to noncuspidal robots. [6], [9]

As a result, path planning algorithms must consider the possibility of nonsingular transitions between solutions, which can lead to unexpected behavior if not properly handled [6], [10]. This is particularly critical in applications requiring high reliability and predictability, such as collaborative human-robot interaction and precision assembly. Given the increasingly common presence of $7R$ robots with wrist sub-chains in humanoid applications, understanding the effects of cuspidality on their kinematics and path planning is critical. To our knowledge, this study is the first comprehensive analysis of cuspidality in redundant robots. The results provide fundamental insights for designing reliable path-planning algorithms and improving the predictability of robot behavior in humanoid and collaborative robotic applications with redundant arms.

I. Organization of the Paper

The remainder of this letter is structured as follows. Section II presents the preliminaries and definitions related to the cuspidality of redundant robots. Section III discusses the kinematic modeling of redundant robots as parameterized $6R$ robots, along with the associated singularity analysis. In Section IV, we present the classification of commercially available redundant robots based on their cuspidality characteristics. Section V delves into the implications of cuspidality in explaining inverse kinematics and its usefulness in the path planning of robots. Finally, Section VI concludes the paper and discusses future research directions toward developing an explainable framework for handling cuspidality and enabling smooth transfer of robot behavior among different platforms.

II. Preliminaries

We start with a set of standard definitions related to the kinematic analysis of nonredundant and redundant robots. The robot parameters are identified by the original Denavit-Hartenberg parameters [11].

Definition 1: An aspect is defined as the largest singularity-free partition in joint space. There exists multiple aspects in a joint space.

Definition 2: The largest semi-algebraic set in the workspace without singularities is defined as a connected component of the workspace. Here, semi-algebraic set refers set of polynomials with inequalities.

Definition 3: *An operation mode* uniquely identifies an inverse kinematic solution (IKS) at any given end-effector pose of a serial robot.

A 2R planar robot has two operation modes: elbow up and elbow down modes. In wrist-partitioned noncuspidal 6R robots, there exist up to eight operation modes that are termed elbow(up/down)-shoulder(right/left)-wrist(flip/unflip) [6]. In a generic $3R$ robot, we can reduce the joint space dimensions to 2 by eliminating θ_1 as it does not define singularities. Similarly, the effect of θ_1 can be removed in the workspace. Thus, a projection of the workspace singularities on a slice of ρ-z, where $\rho = \sqrt{x^2 + y^2}$, can be studied without any loss of information on singularities, as shown in Fig. 2.

Definition 4: A cusp is a point in the workspace of a $3R$ serial robot that satisfies the following conditions [3]:

$$\begin{aligned} M(t) &= 0 \\ \frac{\partial M}{\partial t}(t) &= 0 \\ \frac{\partial^2 M}{\partial t^2}(t) &= 0 \\ \frac{\partial^3 M}{\partial t^3}(t) &\neq 0 \end{aligned} \tag{1}$$

where $M(t)$ is the inverse kinematic polynomial of degree four of a generic $3R$ serial robot, where $t = \tan\frac{\theta_3}{2}$, in Fig. 2, the robot has four cusps located at the corners of the inner region.

Definition 5: The locus of critical values is the image of critical points.

This is commonly termed as singularities in the workspace, and can be derived by solving for $M(t) = 0$, $\frac{\partial M}{\partial t}(t) = 0$ from Eq. (1).

Definition 6: *A cuspidal nonredundant robot* is a robot that has multiple finite IKS in at least one aspect [3].

In cuspidal robots, it is not always feasible to identify every IKS with a unique operation mode. Even if possible, the robot can switch to operating mode without encountering a singular configuration. It was shown in [4] that for any generic $3R$ robot, the existence of a cusp in the critical values of the kinematic function projected onto a $\rho - z$ slice is a necessary and sufficient condition for a robot to be cuspidal. Here, the end-effector position is given as $[x, y, z]^T$ and $\rho = \sqrt{x^2 + y^2}$. An example of a nonsingular change of solution in a $3R$ cuspidal robot with joint space parameterized in $\theta_2 - \theta_3$ and workspace in $\rho - z$ slice is shown in Fig. 2.

Definition 7: A wrist-partitioned 7R robot is a serial robot with seven revolute joints with a subchain of three consecutive joints intersecting at a point (spherical-wrist), either at the beginning or at the end of the architecture. In this letter, we focus on this class of robots and refer to them as redundant robots.

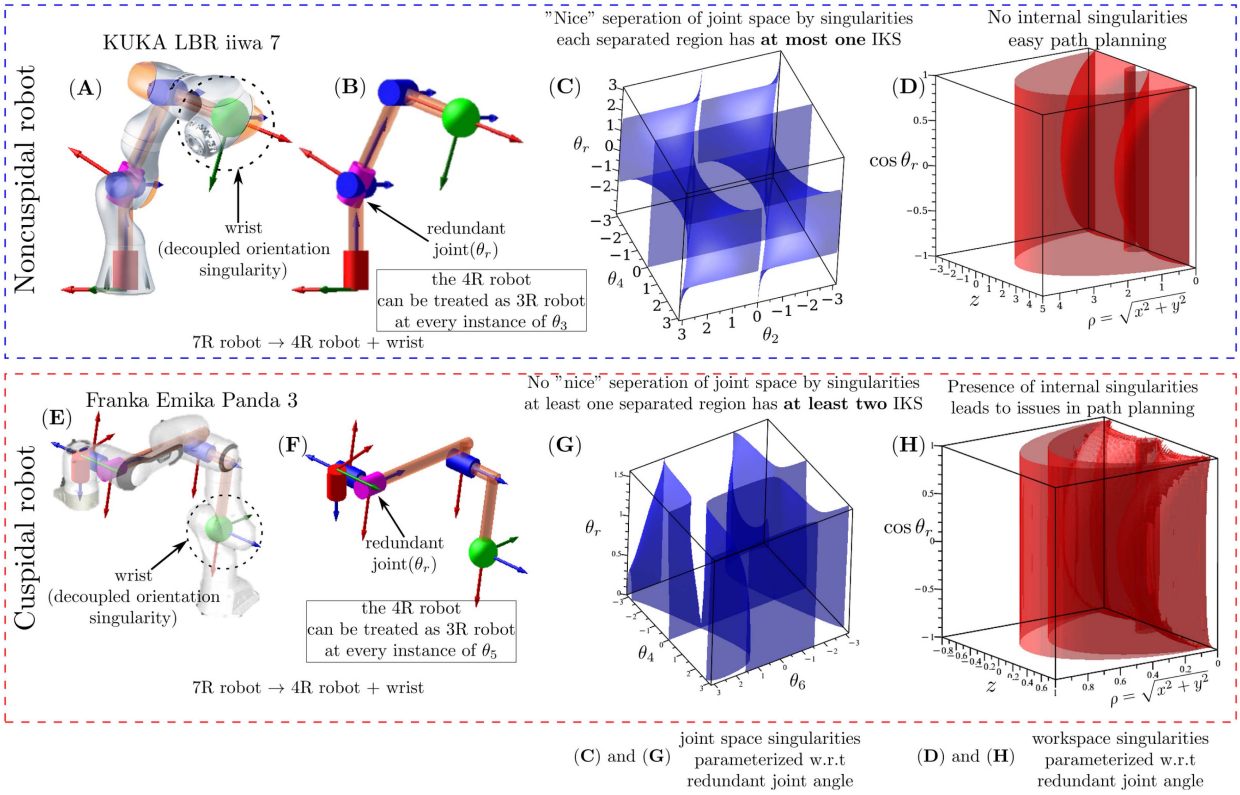

Fig. 1. Comparison of simplified kinematic structure and singularities in joint space and workspace of a commercial noncuspidal and a cuspidal robot. (A-B) The Kuka LWR iiwa robot and its schematic show the decoupling of the last three joints (spherical-wrist) from the rest of the $4R$ position robot. (E-F) Franka Emika Panda 3 robot and schematic of inverted chain showing the decoupling of first three joints (spherical-shoulder) from the rest $4R$ position robot. (C and G) singularities in joint space of the redundant $4R$ noncuspidal and cuspidal robot. (D and H) singularities in the workspace of the redundant $4R$ noncuspidal and cuspidal robot.

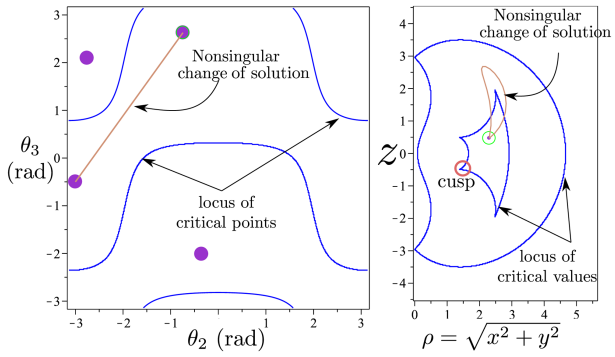

Fig. 2. A nonsingular change of operation modes in joint space and workspace of a cuspidal robot. Robot parameters: d = [0, 1, 0], a = [1, 2, 3/2], $\alpha = [-\frac{\pi}{2}, \frac{\pi}{2}, 0]$. Path in the joint space (θ_2, θ_3): from $(-0.742, 2.628)$ to $(-3, -0.5)$.

Definition 8: A cuspidal redundant robot is a 7R robot with a redundant joint angle θ_r such that for **almost all** values of θ_r, the corresponding 6R robot is cuspidal.

Here, 'almost all' means excluding finite distinct values of θ_r in the $[-\pi, \pi]$ range. For instance, in the example discussed in Section III-B, the $\theta_r \in \{0, \pi, -\pi\}$ are excluded from studying the cuspidal properties as the equivalent mapping from a $7R$ robot to $6R$ robot is singular at these values.

III. Kinematic Analysis

In this section, we discuss the kinematic analysis of the redundant robots and the dimension reduction, allowing one to visualize the singularities of redundant robots. Previously known studies related to inverse kinematic solutions include generalized inverse methods [12], genetic algorithms and particle swarm optimisation [13] as well as closed-form solutions for specific redundant robots [14], [15]. As numerical methods cannot provide all IKS for any given EE-pose, they cannot be employed to study the nature of the distribution of IKS in the joint space.

A redundant wrist-partitioned robot can be decoupled into a redundant positional $4R$ chain and an orientation wrist chain. This is because a wrist can change the orientation of a frame without affecting the position. It was reported earlier [6] that a wrist is a noncuspidal robot as it has two IKS that are separated by a singularity. Thus, the cuspidality of a redundant robot depends only on the redundant positional $4R$ sub-chain.

The redundant angle, θ_r, is one of the joint angles in the positional chain. Every $4R$ serial chain can be mapped to a $3R$ robot for a given value of θ_r. This implies that we can study the singularities of a redundant robot by parameterizing the redundant angle and analyzing the corresponding $3R$ robot. For every value of θ_r, the architecture of the equivalent $3R$ robot changes. Fig. 3 shows the redundant $4R$ positional chain

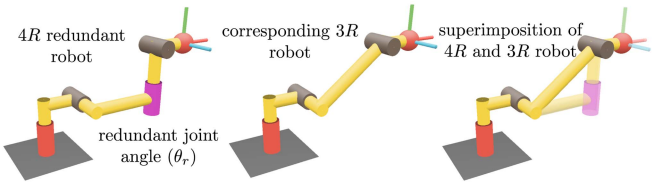

Fig. 3. An example of a $4R$ redundant positional robot (left) and its equivalent $3R$ robot (center) parameterized by the redundant angle (in pink). The rightmost figure shows the superposition of the robots to show the equivalence of the structures.

TABLE II
D-H PARAMETERS FOR A REDUNDANT ROBOT WITH THE SPHERICAL-WRIST

Joint	θ_i	d_i (m)	a_i (m)	α_i
1	θ_1	d_1	a_1	α_1
2	θ_2	d_2	a_2	α_2
3	$\theta_3(\theta_r)$	d_3	a_3	α_3
4	θ_4	d_4	a_4	α_4
5	θ_5	d_5	0	α_5
6	θ_6	0	0	α_6
7	θ_7	d_7	a_7	α_7

and the equivalent $3R$ chain. It can be seen in Fig. 3 that θ_r directly influences the D-H parameter α_2 of the $3R$ robot. As the architecture changes, the global kinematic properties of a given $3R$ robot may change, resulting in internal singularities within the robot's workspace. The advantage of reducing the redundant robot in such a manner is that the cuspidality analysis of the $3R$ robot is well established, and the results from $3R$ robots can be leveraged to understand the joint space and workspace of the redundant robot. It is known that the singularities of the $3R$ robot are independent of the first joint angle, and, thus, the three-dimensional joint space can be projected onto the $\theta_2 - \theta_3$ slice. This dimension reduction now allows us to stack the joint spaces of $3R$ robots with respect to the redundant angle, θ_r, and thus, we obtain complete information on the positional singularities of redundant robots, and the singularities can be visualized in the 3D cartesian space. By doing so, the singularity analysis of the seven-dimensional joint space of a redundant robot can be reduced to a visualised three-dimensional space parameterized in the redundant angle. This further allows us to visualize the singularities in the workspace, too, as shown in Fig. 1(D and H).

A. Redundant Robot With spherical Wrist

Robots that have a spherical-wrist at the end can be studied by decoupling the orientation analysis from the position analysis. The kinematic properties of the $3R$ positional chain can be directly used to extend the results to robots with a spherical-wrist. The kinematics of such a robot can be solved analytically with closed-form solutions.

A $7R$ robot is sometimes parameterized by arm angle as introduced in the past [16], and we will use it to parameterize an example $7R$ robot. The D-H parameters of an example of a redundant robot with aspherical-wrist are given in Table II. As the robot has a spherical-wrist partition, we can decouple the robot and study the $4R$ positional robot separate from the orientation sub-chain. In the robot corresponding to Table II, we take the third angle in the positional chain as the redundant joint angle. Fig. 1(A-B) shows the schematic of the robot and the decoupling of the $7R$ robot as a redundant $4R$ positional chain and a spherical-wrist. The pink joint is treated as the redundant joint, and the red-coloured joint is the first joint of the resulting positional sub-chain. For Kuka iiwa LWR 7, $d_1 = 0.3105, d_2 = d_4 = d_6 = 0, d_3 = 0.4, d_5 = 0.39, d_7 = 0.078, \alpha_1 = \alpha_4 = \alpha_5 = \frac{\pi}{2}, \alpha_2 = \alpha_3 = \alpha_6 = \frac{-\pi}{2}, \alpha_7 = 0, a_i = 0$. The resulting $4R$ chain then can be studied as a $3R$ robot that changes its architecture depending on the value of θ_r. The D-H parameters in Table III can describe the architecture of these $3R$ robots. It is to be noted that as there exists no offset between the first two joints of the robot, the equivalent $3R$ chain only changes the relative joint orientation ($\alpha_2 = \theta_r$ in Table III) while the link lengths and offsets remain constant.

TABLE III
D-H PARAMETERS FOR EQUIVALENT $3R$ CHAIN FOR KUKA IIWA LWR 7 PARAMETERIZED IN THE REDUNDANT ANGLE

Joint	θ_{ri}	d_{ri} (m)	a_{ri} (m)	α_{ri}
1	θ_1	0.3105	0	$\pi/2$
2	θ_2	0	0.4	θ_r
3	θ_4	0	0.39	$-\pi/2$

TABLE IV
D-H PARAMETERS FOR AN EXAMPLE OF A REDUNDANT ROBOT WITH THE WRIST AT THE BEGINNING

Joint	θ_i	d_i (m)	a_i (m)	α_i
1	θ_1	d_1	0	$-\pi/2$
2	θ_2	0	0	$\pi/2$
3	θ_3	d_3	a_3	$\pi/2$
4	θ_4	0	a_4	$-\pi/2$
5	$\theta_5(\theta_r)$	d_5	0	$\pi/2$
6	θ_6	0	a_6	$\pi/2$
7	θ_7	d_7	0	0

B. Redundant Robot With spherical-Shoulder

The kinematic chain for robots with spherical-shoulder can be decoupled in similar fashion as robots with spherical-wrist. In this case, we invert the chain and the position of the centre of the spherical-shoulder with respect to the end-effector frame is treated as the end-effector position. An example of a commercial redundant robot with a spherical-shoulder is the Franka Emika Panda robot. It is used in several applications, including human-robot interaction [17]. The D-H parameters of the robot are given in Table IV where, $d_1 = 0.333, d_3 = 0.316, d_5 = 0.384, d_7 = 0.107, a_3 = 0.0825, a_4 = -0.0825, a_6 = 0.088$. Fig. 1(E-F) shows the schematic of the Panda robot and the decoupling of the $7R$ robot as an inverted redundant $4R$ chain and a spherical-shoulder. In this robot, the fifth joint angle is treated as the redundant joint angle, and an equivalent $3R$ chain for the redundant $4R$ positional chain is found by parameterizing the redundant angle.

Fig. 4 illustrates the process of decoupling the positional sub-chain and the resulting equivalent $3R$ chain. In this robot, a significant difference is the offset $a_6 \neq 0$ at the end of the robot.

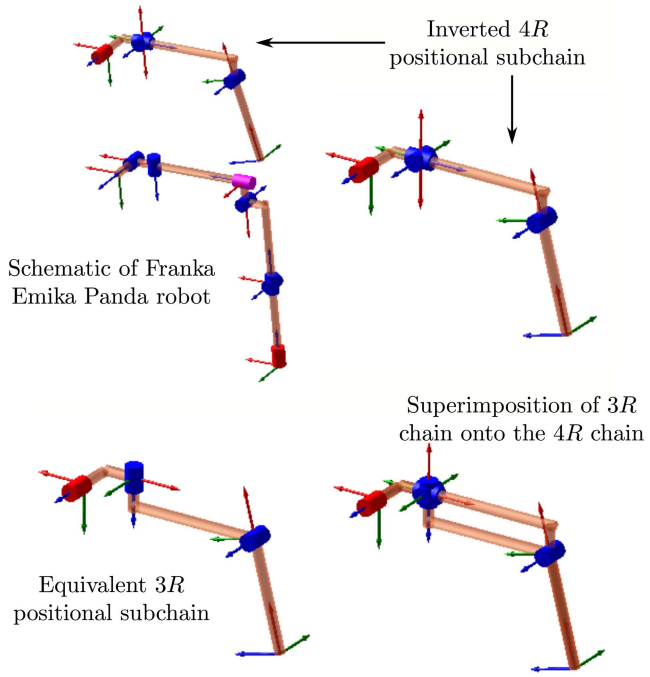

Fig. 4. The schematic for decoupling the spherical-shoulder from the positional $4R$ robot (top). The redundant robot is then decoupled in an equivalent $3R$ robot parameterized by the redundant angle (bottom).

TABLE V
D-H PARAMETERS FOR EQUIVALENT $3R$ CHAIN FOR FRANKA EMIKA PANDA ROBOT

Joint	θ_{r_i}	d_{r_i} (m)	a_{r_i} (m)	α_{r_i}
1	θ_{r_1}	$-d_7$	$-a_6$	$-\frac{\pi}{2}$
2	θ_{r_2}	$\frac{a_3}{\sin(\theta_r)}$	d_5	$\theta_r - \pi$
3	θ_{r_3}	$\frac{a_3\cos(\theta_r)}{\sin(\theta_r)}$	$-\sqrt{a_3^2+d_3^2}$	$-\frac{\pi}{2}$

This offset introduces major kinematic changes in the robot from the anthropomorphic robots discussed in Section III-A. Because of this joint offset, the equivalent $3R$ chain has varying link lengths (d and a values) and changing joint arrangements (α values). As the $4R$ positional chain has been inverted, we denote the i^{th} joint angle of the chain with r_i (here, r implies a reversed order and not a redundant angle). The architecture of the equivalent $3R$ chain can be defined by following D-H parameters in Table V.

It can be seen that the mapping between $4R$ chain and its equivalent $3R$ chain is singular at $\theta_r \in \{0, \pm\pi\}$ as $\sin(\theta_r)$ appears in the denominator. For these singular values, the equivalent $3R$ chain can be re-defined with $\mathbf{a} = [-a_6, \sqrt{d_5^2 + a_4^2}, -\sqrt{a_3^2 + d_3^2}]$, $\mathbf{d} = [d_7, 0, 0]$ and adding an offset in the joint angles $\theta = [\theta_{r_1}, \theta_{r_2} + arctan(\frac{a_4}{d_5}), \theta_{r_3} + arctan(\frac{a_4}{d_5})]$.

Fig. 5 shows how the links in the equivalent $3R$ chain increase as θ_r approaches 0 radians. As shown in this section, an offset in joints may alter the robot's kinematic properties. As human-robot interaction gains popularity, new designs are introduced for redundant robots, leading to a deviation from original anthropomorphic designs, and thus, it is necessary to study these designs for cuspidality.

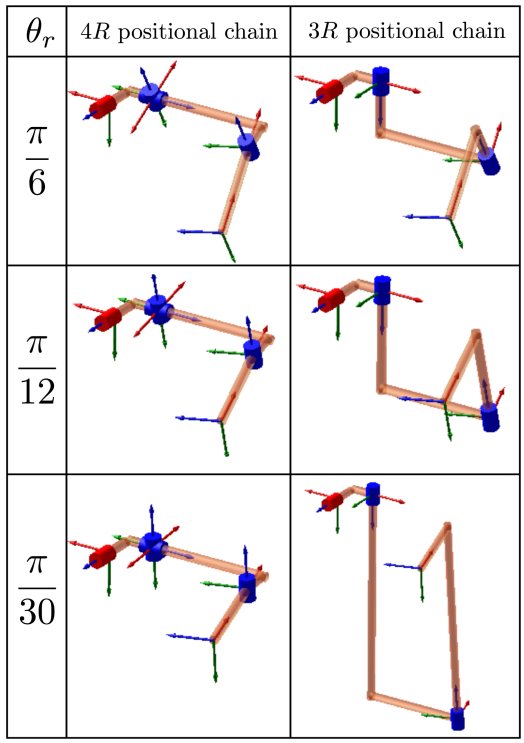

Fig. 5. Inverted $4R$ positional robot in Franka Emika Panda robot and the equivalent $3R$ chain for different values of the redundant angle θ_r.

IV. SINGULARITY VISUALIZATION AND CLASSIFICATION

In this section, the classification of the redundant robots based on cuspidal properties is discussed. As discussed in Section III, the kinematic analysis of redundant robots can be studied by using the reduced equivalent mapping to a $3R$ robot. The same applies to the singularities in joint space and the workspace. The singularities and cuspidal properties for a generic $3R$ robot are well documented in the past [4], [18], [19], [20] allowing us to leverage the previously known results to classify redundant robots too.

A. Noncuspidal Redundant Robot

A noncuspidal redundant robot is a robot whose reduced $3R$ robot can be classified as noncuspidal at every value of the redundant joint angle θ_r. It has been reported earlier that if the first two joints are intersecting, the resulting $3R$ positional chain is noncuspidal [21]. We discuss a noncuspidal redundant robot by specifically using this result by considering the KUKA iiwa LWR robot which has this architecture. Fig. 6 shows the singularities in joint space at four different values of the redundant angle, viz, $\frac{\pi}{12}, \frac{\pi}{6}, \frac{\pi}{3}, \frac{\pi}{2}$ for an example of a noncuspidal redundant robot. The end effector position chosen is [0, 0.2, -0.3], and the IKS for each value of θ_r is shown in this figure. It can be confirmed that all the slices have 4 IKS, and each is separated into four aspects by singularities. The direct

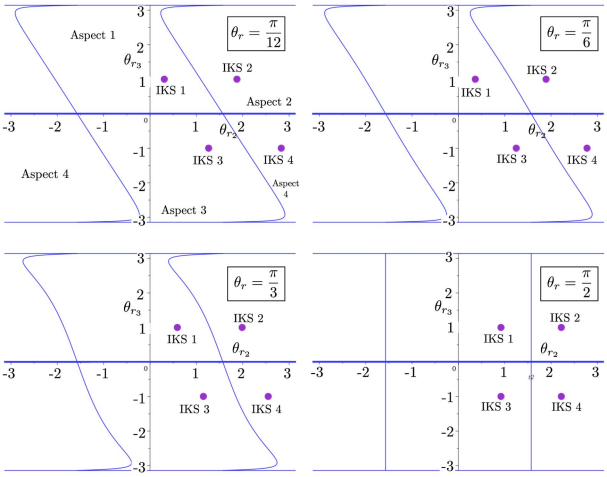

Fig. 6. Singularities in the joint space and the distribution of IKS for KUKA iiwa LWR for discrete slices parametrized by θ_r. It can be seen that at each value of θ_r, the singularities well separate the four IKS, and a nonsingular change of operation mode is thus not possible. This suggests that the robot is noncuspidal.

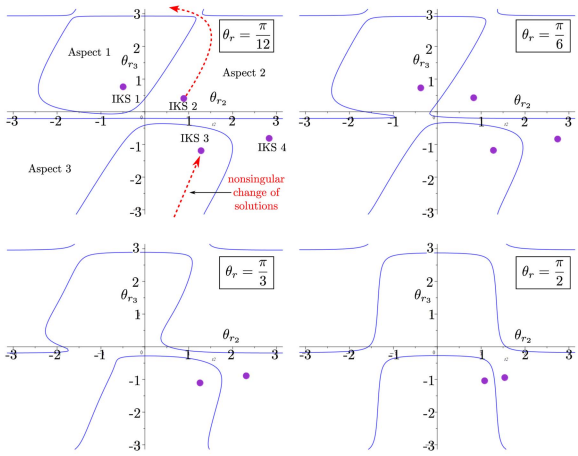

Fig. 8. Singularities in the joint space and the distribution of IKS for Franka Emika Panda robot for discrete slices parameterized by θ_r.It can be seen that at each value of θ_r, there exist only two aspects in the joint space but four IKS, and a nonsingular change of operation mode is thus possible. This shows that the robot is cuspidal.

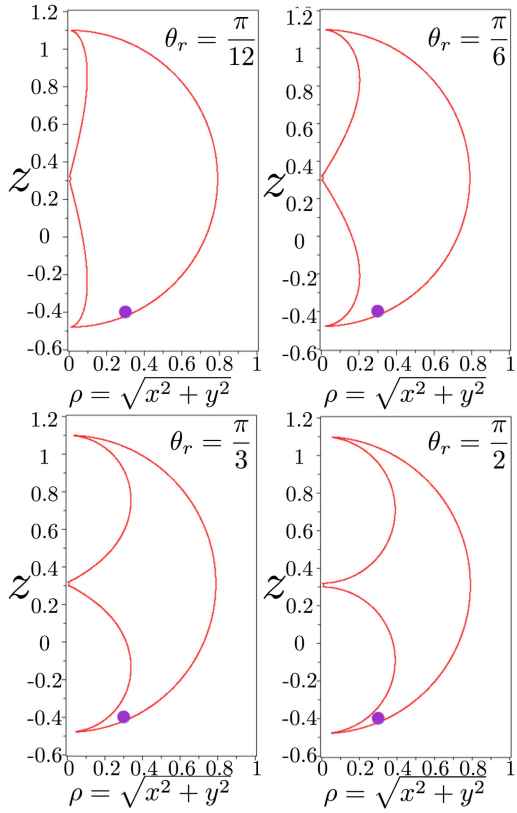

Fig. 7. Locus of critical values of KUKA iiwa LWR for discrete slices of θ_r. There are no internal singularities, nodes, or cusps in the workspace slice, which suggests simplified kinematics.

implication of this separation is identifying each class of IKS for each value of θ_r. In theory, we have infinite solutions for the end-effector position as we have a redundant angle present in the positional chain, but at every value of θ_r, we can identify the operation mode of the robot by identifying the aspect in the joint space. The aspect of the robot uniquely identifies each operation mode, and as the joint space is parameterized in θ_r, it allows one to study the operation modes of a redundant robot at any given joint configuration.

B. *Cuspidal Redundant Robot*

A cuspidal redundant robot is defined as a $7R$ manipulator for which the reduced $3R$ chain exhibits cuspidal behaviour for almost all values of the redundant joint angle θ_r. In other words, a nonsingular change of inverse kinematic solutions (IKS) within the same aspect of the joint space, even though the robot is kinematically redundant. This property introduces critical challenges in motion planning, as the robot may switch between operation modes during continuous motion without passing through a singularity, undermining the predictability of the IKS evolution.

To illustrate this behaviour, we consider the Franka Emika Panda robot, a commercially available 7R wrist-partitioned manipulator with the spherical-shoulder in the kinematic chain. As shown in Fig. 4, the robot is decoupled into an inverted 4R positional sub-chain and a spherical-wrist for orientation. By treating the fifth joint as the redundant joint, an equivalent 3R chain can be derived by parameterizing θ_r. The resulting D-H parameters for the equivalent 3R chain are provided in Table V.

Fig. 8 demonstrates the singularities in the joint space for discrete values of θ_r. Unlike the noncuspidal case, these slices reveal multiple IKS within singularity-free regions, confirming the presence of nonsingular transitions between operation modes—i.e., cuspidality. Additionally, Fig. 9 shows the critical value locus in the workspace, which exhibits a cusp in the curves, thus confirming the cuspidal nature of the robot. The effect of the offset $a_6 \neq 0$ in the Franka robot amplifies the complexity of the equivalent $3R$ kinematic structure, allowing it to satisfy the cusp condition.

The presence of such behaviour in a widely used collaborative robot underscores the importance of incorporating cuspidality

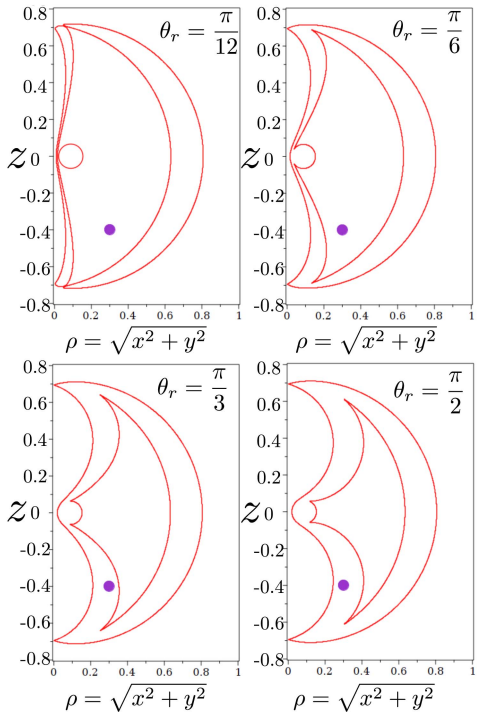

Fig. 9. Locus of the critical value of Franka Emika Panda robot for discrete slices of θ_r.The workspace has internal singularities and cusps in the workspace, thus showing a more complicated kinematics than the noncuspidal robot shown in Fig. 7.

analysis into both the design and control pipeline of redundant manipulators. While redundancy offers an infinite number of configurations for a given end-effector pose, it does not inherently guarantee safe or predictable transitions between these configurations, especially in cuspidal robots.

V. Discussion

In this section, we discuss the nonsingular change of solutions in a redundant cuspidal robot and provide a brief guideline for designing a noncuspidal redundant robot.

A. Nonsingular Change of Solutions

This section demonstrates a nonsingular change of inverse kinematic solutions (IKS) in the *modified* redundant 7-degree-of-freedom robot Motoman SIA5D (refer to Fig. ??(left)) by illustrating a continuous transition between different configurations without encountering a singularity. The D-H parameters of the example robot are provided in Table VI, and a key observation is that the offset $d_2 \neq 0$ plays a crucial role in making the robot cuspidal when $a_1 \neq 0$. This non-zero offset, d_2, leads to the existence of a cusp in the configuration space, a defining characteristic of cuspidal robots that allows them to switch between different IKS branches without passing through a singularity. This depicts a *closed path* in the Cartesian workspace that encircles the cusp in workspace and corresponds to a *open path* in joint space that changes IKS, confirming a nonsingular change of solutions. It is to be noted that this example is provided solely for illustrative purposes of a nonsingular change in solution in a redundant robot. The Motoman SIA5D has $a_1 = 0$, which makes the robot noncuspidal. The above example was chosen to illustrate that as new designs are introduced commercially, it is crucial to understand the implications of each offset, as even a small value may alter the overall kinematic properties of the robot.

TABLE VI
D-H Parameters for Modified Motoman SIA5D Robot ($a_1 \neq 0$)

Joint	θ_i	d_i (mm)	a_i (mm)	α_i
1	θ_1	310	50	$-\pi/2$
2	θ_2	0	0	$\pi/2$
3	$\theta_3(\theta_r)$	270	85	$\pi/2$
4	θ_4	0	60	$-\pi/2$
5	θ_5	270	0	$\pi/2$
6	θ_6	0	0	$\pi/2$
7	θ_7	145	0	0

TABLE VII
List of Few Commercial 7R Robots Classified by the Cuspidal Properties

Robot	**Year**	**wrist/shoulder**	**Classification**
Maira (Neura Robotics)	2024	yes, yes	Noncuspidal
Franka Research 3	2022	no, yes	Cuspidal
Unitree G1 Arm	2023	no, yes	Noncuspidal
Motoman SIA5D	2022	yes, yes	Noncuspidal
xArm7	2022	no, yes	Noncuspidal
Motoman SIA50D	2022	yes, no	Noncuspidal
Diana 7 (Agile Robotics)	2019	no, yes	Cuspidal
Rizon 7 (Flexiv Robotics)	2019	no, no	N.A.
KR810 (Kassow Robotics)	2019	no, no	N.A.
KUKA LWR iiwa	2013	yes, yes	Noncuspidal
Barrett WAM	1990	yes, no	Noncuspidal
Motoman SIA50D ($a_3 \neq 0$)	-	yes, no	Cuspidal
Motoman SIA5D ($a_1 \neq 0$)	-	yes, no	Cuspidal

B. Guidelines to Design Noncuspidal Redundant Robots

This study demonstrates that the inclusion of offsets in joint parameters of redundant 7R robots can significantly influence their kinematic behaviour, potentially making them cuspidal. A key implication of cuspidality in redundant robots is that, despite having infinitely many inverse kinematic solutions (IKS) as a function of the redundant joint angle, the robot may still exhibit feasibility and repeatability challenges in motion planning. These issues arise because cuspidal robots allow nonsingular transitions between IKS, rendering path planning less predictable and increasing the risk of unintended assembly mode switches. We illustrate this in Table VII summarizing several commercially available redundant robots and their cuspidal classifications. Almost all $7R$ robots are derived as extensions of existing $6R$ counterparts developed by the parent company. Many modern $6R$ cobots—engineered to enable safe and flexible human-robot interaction—naturally exhibit cuspidal characteristics due to their design choices. While such architectures provide enhanced dexterity, they can introduce complexities in motion planning. In contrast, noncuspidal robots offer a more predictable and interpretable kinematic structure, which can be especially advantageous in applications demanding high

repeatability and reliability. This highlights the value of systematically understanding and, where possible, favoring noncuspidal designs for redundant robots, particularly in collaborative robotics. To support designers in this direction, we propose a set of practical guidelines for constructing noncuspidal redundant robots:

1) Prefer anthropomorphic design of $7R$ robot, that is, a spherical-shoulder and a spherical-wrist with the third joint intersecting both second and fourth joint (existing examples: KUKA IIWA LWR 7, 14).
2) If there exists an offset between the third and fourth joint, then make sure that a spherical-wrist exists and the first two joints intersect ($a_1 = 0$), such as Motoman SIA5D.
3) If there exists an offset in the first two joints ($a_1 \neq 0$), then make sure that a spherical-wrist exists and the third joint intersects both the second and fourth joint (existing examples: Motoman SIA50D).
4) Prefer intersecting joints over adding offsets, but if an offset is required for manipulation purposes, design curved links to maintain a spherical-wrist configuration, such as the MaiRa robot from Neura Robotics.

VI. Conclusion

In this work, we presented a systematic framework for analyzing the cuspidality of redundant 7R robots by reducing their kinematic structure to parameterized 3R equivalents through the redundant joint angle. This approach enabled us to leverage the well-established theory of cuspidal behaviour in 3R manipulators to classify the global kinematic properties of more complex redundant architectures. Our analysis revealed that many commercially available redundant robots—particularly cobots—are inherently cuspidal due to design offsets, which can lead to unexpected nonsingular transitions between inverse kinematic solutions. Such behaviour complicates path planning, especially in applications demanding high reliability and repeatability. To the best of our knowledge, this is the first comprehensive study to address cuspidality in redundant robots and highlight its practical implications. This foundational insight opens the door to developing new, cuspidality-aware planning and control strategies that can enhance the predictability and safety of next-generation robotic systems. This study is limited to wrist-partitioned robots with revolute joints, where orientation and positional sub-chain decouple, allowing workspace reduction. For non-wrist-partitioned 6R robots, no necessary and sufficient condition for cuspidality exists, only partial criteria [6]. The topological methods used for singularity analysis do not apply to prismatic joints; therefore, different methods are required for cuspidality analysis of such robots. Moving forward, this understanding should inform both controller design and robot architecture, with future research focusing on developing path-planning strategies that are explicitly aware of cuspidality to guarantee safe and repeatable operation even in complex, high-DOF systems.

References

[1] B. Siciliano, "A closed-loop inverse kinematic scheme for on-line joint-based robot control," *Robotica*, vol. 8, no. 3, pp. 231–243, 1990.

[2] D. H. Salunkhe, D. Chablat, and P. Wenger, "Trajectory planning issues in cuspidal commercial robots," in *Proc. IEEE Int. Conf. Robot. Automat.*, 2023, pp. 7426–7432.

[3] J. El Omri and P. Wenger, "How to recognize simply a non-singular posture changing 3-DoF manipulator," in *Proc. 7th Int. Conf. Adv. Robot.*, 1995, pp. 215–222.

[4] D. H. Salunkhe, C. Spartalis, J. Capco, D. Chablat, and P. Wenger, "Necessary and sufficient condition for a generic 3r serial manipulator to be cuspidal," *Mechanism Mach. Theory*, vol. 171, Jan. 2022, Art. no. 104729.

[5] D. Salunkhe, J. Capco, D. Chablat, and P. Wenger, "Geometry based analysis of 3R serial robots," in *Advances in Robot Kinematics*, O. Altuzarra and A. Kecskeméthy, Eds. Cham, Switzerland: Springer, 2022, pp. 65–72.

[6] D. H. Salunkhe, T. Marauli, A. Müller, D. Chablat, and P. Wenger, "Kinematic issues in 6R cuspidal robots, guidelines for path planning and deciding cuspidality," *Int. J. Robot. Res.*, vol. 44, pp. 1035–1054, 2024.

[7] M. Asgari, I. Bonev, and C. Gosselin, "Singularities of ABB's YuMi 7-DoF robot arm," *Mechanism Mach. Theory*, vol. 205, 2025. [Online]. Available: https://www.sciencedirect.com/science/article/pii/S0094114X24003112

[8] A. J. Elias and J. T. Wen, "Redundancy parameterization and inverse kinematics of 7-DoF revolute manipulators," *Mechanism Mach. Theory*, vol. 204, 2024, Art. no. 105824.

[9] P. Wenger, "Uniqueness domains and regions of feasible paths for cuspidal manipulators," *IEEE Trans. Robot.*, vol. 20, no. 4, pp. 745–750, Aug. 2004.

[10] A. J. Elias and J. T. Wen, "Path planning and optimization for cuspidal 6R manipulators," ASME. *J. Mechanisms Robot.*, vol.17, no. 12, Dec. 2025, Art. no. 121008, doi: 10.1115/1.4069599.

[11] J. Denavit and R. S. Hartenberg, "A kinematic notation for lower-pair mechanisms based on matrices," *J. Appl. Mechan.*, vol. 22, no. 2, pp. 215–221, 1955.

[12] J. Demby's, J. Uhlmann, and G. N. DeSouza, "Choosing the correct generalized inverse for the numerical solution of the inverse kinematics of incommensurate robotic manipulators," 2023, *arXiv:2308.02954*.

[13] P. Monfared, X. Fei, and W. Peng, "Computation of inverse kinematics of redundant manipulator using particle swarm optimization algorithm and its combination with artificial neural networks," *Eng. Proc.*, vol. 76, no. 1, 2024, Art. no. 58.

[14] M. Pfurner, "Closed form inverse kinematics solution for a redundant anthropomorphic robot arm," *Comput. Aided Geometric Des.*, vol. 47, pp. 163–171, 2016.

[15] S. Wang, Z. Liu, Z. Ma, H. Chang, P. Huang, and Z. Lu, "A closed-form solution for inverse kinematics of redundant space manipulator with multiple joint offsets," *Adv. Space Res.*, vol. 72, no. 5, pp. 1844–1860, 2023. [Online]. Available: https://www.sciencedirect.com/science/article/pii/S0273117723003563

[16] M. Gong, X. Li, and L. Zhang, "Analytical inverse kinematics and self-motion application for 7-DOF redundant manipulator," *IEEE Access*, vol. 7, pp. 18662–18674, 2019.

[17] S. Haddadin, "The Franka Emika robot: A standard platform in robotics research [Survey]," *IEEE Robot. Autom. Mag.*, vol. 31, no. 4, pp. 136–148, Dec. 2024.

[18] J. W. Burdick, "On the inverse kinematics of redundant manipulators: Characterization of the self-motion manifolds," in *Proc. Int. Conf. Adv. Robot.*, 1989, pp. 25–34.

[19] D. Paganelli, "Topological analysis of singularity loci for serial and parallel manipulators," Ph.D. dissertation, Dept. Mechanics applied machinesUniv. di Bologna, Bologna, Italy, 2008.

[20] P. Wenger, "Classification of 3R positioning manipulators," *J. Mech. Des.*, vol. 120, no. 2, pp. 327–332, 1998.

[21] P. Wenger and D. Chablat, "A review of cuspidal serial and parallel manipulators," *J. Mechanisms Robot.*, vol. 15, no. 4, 2022, Art. no. 040801.